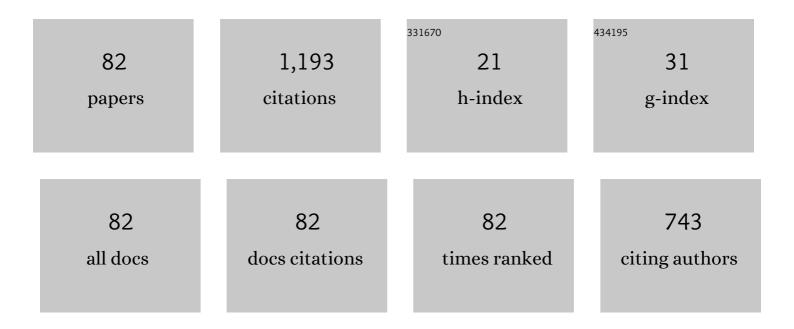
List of Publications by Year in descending order

Source: https://exaly.com/author-pdf/1172833/publications.pdf Version: 2024-02-01



Οινς-Ζηι Υλν

#	Article	lF	CITATIONS
1	Large-scale potassium-doped tungsten alloy with superior recrystallization resistance, ductility and strength induced by potassium bubbles. Journal of Nuclear Materials, 2022, 559, 153450.	2.7	20
2	Microstructure stability, softening temperature and strengthening mechanism of pure copper, CuCrZr and Cu-Al2O3 up to 1000 â,,f. Nuclear Materials and Energy, 2022, 30, 101123.	1.3	5
3	Synergistic effects of Si and Y on corrosion behavior of cast cladding steels by pre-laying Y powder for nuclear applications in static liquid LBE. Journal of Nuclear Materials, 2022, 566, 153781.	2.7	11
4	Microstructure and high temperature mechanical properties of the new cladding steel of 15Cr-15Ni-Ti-Y. Nuclear Materials and Energy, 2022, 31, 101200.	1.3	1
5	Comprehensive analysis of the cladding tubes manufactured by a new 10Cr1SiY ferrite/martensitic steel. Nuclear Materials and Energy, 2022, 32, 101206.	1.3	1
6	Surface modification and deuterium retention in hot-rolled potassium doped tungsten alloy exposed to deuterium plasma. Journal of Nuclear Materials, 2022, 568, 153890.	2.7	4
7	Role of titanium carbide and alumina on the friction increment for Cu-based metallic brake pads under different initial braking speeds. Friction, 2021, 9, 1543-1557.	6.4	15
8	Siâ€rich pressureless sintering of the gelcasted Ti 3 SiC 2 bulk ceramic. International Journal of Applied Ceramic Technology, 2021, 18, 1542-1552.	2.1	0
9	The wet braking and recovery behaviors of the P/M pad mated with C/C–SiC disc for high-speed trains. Wear, 2021, 468-469, 203609.	3.1	7
10	The investigation of distribution on size and concentration of helium bubbles in Y-bearing ODS steel using by SAXS and GIXRD. Journal of Nuclear Materials, 2021, 554, 153083.	2.7	4
11	Preparation of hot-rolled potassium doped tungsten (KW) thick plate and performance of KW-Cu monoblock mock-ups under high heat flux testing. Nuclear Materials and Energy, 2020, 23, 100744.	1.3	4
12	Ti2AlC bulk ceramics produced by gelcasting and Al-rich pressureless sintering. Ceramics International, 2020, 46, 14767-14775.	4.8	4
13	The braking behaviors of Cu-Based powder metallurgy brake pads mated with C/C–SiC disk for high-speed train. Wear, 2020, 448-449, 203237.	3.1	25
14	Preparation of Ti3AlC2 bulk ceramic via aqueous gelcasting followed by Al-rich pressureless sintering. Journal of the European Ceramic Society, 2020, 40, 2878-2886.	5.7	6
15	Effects of yttrium oxides on the microstructure and mechanical properties of 15-15Ti ODS alloy fabricated by casting. Materials Characterization, 2020, 162, 110228.	4.4	10
16	Homogeneity analysis of Y-bearing 12Cr ferritic/martensitic steel fabricated by vacuum induction melting and casting. Journal of Iron and Steel Research International, 2020, 27, 940-951.	2.8	1
17	Fabrication and mechanical properties of largeâ€scale SiC impeller via vacuum gelcasting and pressureless sintering. International Journal of Applied Ceramic Technology, 2020, 17, 1713-1722.	2.1	5
18	Microstructure and strengthening mechanism of grain boundary strengthened W-ZrB2 alloy. Journal of Materials Research and Technology, 2020, 9, 4007-4015.	5.8	17

#	Article	IF	CITATIONS
19	Steam oxidation behavior of Y-bearing cladding tube with aluminizing coating. Materials Research Express, 2020, 7, 066515.	1.6	1
20	Composition, microstructure and mechanical homogeneity evaluation of the Y-bearing 9Cr F/M steel fabricated by VIM & casting technique. Materials Research Express, 2020, 7, 036518.	1.6	1
21	Preparation of large-scale Ti3SiC2 ceramic impeller with complex shape basing on the optimization of sintering manner. Ceramics International, 2019, 45, 22308-22315.	4.8	5
22	Improvement of wear resistance in ferrite-pearlite railway wheel steel via ferrite strengthening and cementite spheroidization. Materials Research Express, 2019, 6, 106513.	1.6	13
23	Grain boundary strengthened W-ZrB2 alloy via freeze-drying technique and spark plasma sintering. Fusion Engineering and Design, 2019, 149, 111333.	1.9	8
24	Microstructure characteristics and properties of yttrium-bearing 9Cr ferritic-martensitic steel cladding tubes. Materials Research Express, 2019, 6, 0965c6.	1.6	3
25	Preparation of a diamond coating by the CVD method on the tungsten substrate and its resistance to D plasma irradiation. Tungsten, 2019, 1, 178-184.	4.8	0
26	Wear behavior of metal bond diamond composite with hollow spherical silica particles as pore former. International Journal of Advanced Manufacturing Technology, 2019, 104, 4757-4767.	3.0	4
27	Characterization of Y-bearing particles in CNS-I-ODS steel fabricated by vacuum induction melting & casting technique. Journal of Materials Research and Technology, 2019, 8, 3859-3871.	5.8	3
28	Enhanced creep resistance of Y-bearing 9Cr ferritic/martensitic steel via vacuum casting technique. Journal of Materials Research and Technology, 2019, 8, 4588-4597.	5.8	6
29	Hardness matching of rail/wheel steels for high-speed-train based on wear rate and rolling contact fatigue performance. Materials Research Express, 2019, 6, 066501.	1.6	4
30	The preparation of TiC dispersion strengthened tungsten alloy via freeze-drying method. Materials Research Express, 2019, 6, 1165g7.	1.6	6
31	Hardness ratio optimization of HiSi wheel/U71MnG rail tribo-pairs by sliding wear for high-speed train. Materials Research Express, 2019, 6, 1265b3.	1.6	1
32	A new method for preparing 9Cr-ODS steel using elemental yttrium and Fe2O3 oxygen carrier. Journal of Alloys and Compounds, 2019, 770, 831-839.	5.5	31
33	Microstructure characteristics of 12Cr ferritic/martensitic steels with various yttrium additions. Journal of Rare Earths, 2019, 37, 547-554.	4.8	19
34	Achievement of high strength-ductility combination in railway wheel steel with thin pearlite and spherical cementite via composition and undercooling design. Materials Research Express, 2019, 6, 016546.	1.6	3
35	Stability of Metal Matrix Composite Pads During High-Speed Braking. Tribology Letters, 2018, 66, 1.	2.6	40
36	The Influence of Cu/Fe Ratio on the Tribological Behavior of Brake Friction Materials. Tribology Letters, 2018, 66, 1,	2.6	55

#	Article	IF	CITATIONS
37	Preparation of W–TiC alloys from core–shell structure powders synthesized by an improved wet chemical method. Rare Metals, 2018, , 1.	7.1	1
38	Low-cost solid FeS lubricant as a possible alternative to MoS2 for producing Fe-based friction materials. International Journal of Minerals, Metallurgy and Materials, 2017, 24, 115-121.	4.9	10
39	Preparation of pure tungsten via various rolling methods and their influence on macro-texture and mechanical properties. Materials and Design, 2017, 126, 1-11.	7.0	33
40	Microstructures, Mechanical Properties and Thermal Conductivities of W-0.5Âwt.%TiC Alloys Prepared via Ball Milling and Wet Chemical Method. Jom, 2017, 69, 1992-1996.	1.9	10
41	Effects of TiC content on microstructure, mechanical properties, and thermal conductivity of W-TiC alloys fabricated by a wet-chemical method. Fusion Engineering and Design, 2017, 121, 366-372.	1.9	25
42	The Braking Behaviors of Cu-Based Metallic Brake Pad for High-Speed Train Under Different Initial Braking Speed. Tribology Letters, 2017, 65, 1.	2.6	75
43	Nanostructured laminar tungsten alloy with improved ductility by surface mechanical attrition treatment. Scientific Reports, 2017, 7, 1351.	3.3	13
44	Creep behaviors and microstructure analysis of CNS-2 steel at elevated temperatures and stresses. Journal of Nuclear Materials, 2017, 495, 306-313.	2.7	4
45	Solid FeS lubricant: a possible alternative to MoS2 for Cu–Fe-based friction materials. International Journal of Minerals, Metallurgy and Materials, 2017, 24, 1278-1283.	4.9	9
46	Microstructures, Mechanical Properties and Deuterium Blistering Behavior of Chemically Prepared W–TiC Alloys. Journal of Fusion Energy, 2017, 36, 71-79.	1.2	7
47	Recrystallization temperature of tungsten with different deformation degrees. Rare Metals, 2016, 35, 566-570.	7.1	25
48	Effect of the pouring temperature by novel synchronous rolling-casting for metal on microstructure and properties of ZLI04 alloy. Journal of Materials Research, 2016, 31, 2524-2530.	2.6	7
49	Nanocrystalline-grained tungsten prepared by surface mechanical attrition treatment: Microstructure and mechanical properties. Journal of Nuclear Materials, 2016, 480, 281-288.	2.7	12
50	Evolution of hot rolling texture in pure tungsten and lanthanum oxide doped tungsten with various reductions. Materials and Design, 2016, 109, 443-455.	7.0	20
51	Effect of stirring velocity in micro fused-casting for metal on microstructure and mechanical properties of A356 aluminum alloy slurry. Journal Wuhan University of Technology, Materials Science Edition, 2016, 31, 1131-1136.	1.0	1
52	Thermal Shock Performance of Sintered Pure Tungsten with Various Grain Sizes Under Transient High Heat Flux Test. Journal of Fusion Energy, 2016, 35, 666-672.	1.2	4
53	Microstructure, basic thermal–mechanical and Charpy impact properties of W-0.1Âwt.% TiC alloy via chemical method. Journal of Alloys and Compounds, 2016, 660, 184-192.	5.5	33
54	Preparation and microstructure characterization of W–0.1wt.%TiC alloy via chemical method. International Journal of Refractory Metals and Hard Materials, 2016, 55, 33-38.	3.8	27

#	Article	IF	CITATIONS
55	Texture evolution and basic thermal–mechanical properties of pure tungsten under various rolling reductions. Journal of Nuclear Materials, 2016, 468, 339-347.	2.7	37
56	Void swelling in ferritic-martensitic steels under high dose ion irradiation: Exploring possible contributions to swelling resistance. Scripta Materialia, 2016, 112, 9-14.	5.2	38
57	A simple way to prepare silicon carbide reinforced graphite composite lubricating materials. Journal Wuhan University of Technology, Materials Science Edition, 2015, 30, 288-291.	1.0	5
58	Void swelling in high dose ion-irradiated reduced activation ferritic–martensitic steels. Journal of Nuclear Materials, 2015, 462, 119-125.	2.7	47
59	Effect of substrate movement speed by synchronous rolling-casting freeform manufacturing for metal on microstructure and mechanical property of ZL104 aluminum alloy slurry. Journal Wuhan University of Technology, Materials Science Edition, 2015, 30, 1056-1060.	1.0	5
60	Comparison of Friction and Wear Behavior Between C/C, C/C-SiC and Metallic Composite Materials. Tribology Letters, 2015, 60, 1.	2.6	28
61	Effect of helium implantation on SiC and graphite. Chinese Physics B, 2015, 24, 037803.	1.4	3
62	The Stability of the Coefficient of Friction and Wear Behavior of C/C–SiC. Tribology Letters, 2015, 58, 1.	2.6	20
63	The influence of microstructure on the rolling contact fatigue of steel for high-speed-train wheel. Wear, 2015, 342-343, 349-355.	3.1	30
64	Effects of temperature induced thermal expansion and oxidation on the Charpy impact property of C/C composites. Journal Wuhan University of Technology, Materials Science Edition, 2015, 30, 473-477.	1.0	2
65	Thermal/mechanical properties of short carbon fibre/SiC coâ€reinforced graphite matrix composites produced by low temperature hot pressing. Micro and Nano Letters, 2015, 10, 263-266.	1.3	1
66	Fabrication of solid-phase-sintered SiC-based composites with short carbon fibers. International Journal of Minerals, Metallurgy and Materials, 2014, 21, 1141-1145.	4.9	4
67	The thermal crack characteristics of rolled tungsten in different orientations. Journal of Nuclear Materials, 2014, 444, 428-434.	2.7	28
68	The influence of granulation on the gelcasting of pressureless-sintered silicon carbide ceramics. Ceramics International, 2014, 40, 7245-7251.	4.8	5
69	Thermal shock and fatigue resistance of tungsten materials under transient heat loading. Journal of Nuclear Materials, 2014, 455, 537-543.	2.7	22
70	Microstructure, mechanical properties and bonding characteristic of deformed tungsten. International Journal of Refractory Metals and Hard Materials, 2014, 43, 302-308.	3.8	18
71	Basic thermal–mechanical properties and thermal shock, fatigue resistance of swaged+rolled potassium doped tungsten. Journal of Nuclear Materials, 2014, 452, 257-264.	2.7	22
72	Morphology evolution of La2O3 and crack characteristic in W–La2O3 alloy under transient heat loading. Journal of Nuclear Materials, 2014, 451, 283-291.	2.7	25

QING-ZHI YAN

#	Article	IF	CITATIONS
73	Effect of hot working process on the mechanical properties of tungsten materials. Journal of Nuclear Materials, 2013, 442, S233-S236.	2.7	43
74	Sintering behavior of Cr in different atmospheres and its effect on the microstructure and properties of copper-based composite materials. International Journal of Minerals, Metallurgy and Materials, 2013, 20, 1208-1213.	4.9	9
75	Bulk tungsten with uniformly dispersed La2O3 nanoparticles sintered from co-precipitated La2O3/W nanoparticles. Journal of Nuclear Materials, 2013, 434, 85-89.	2.7	61
76	Hot Deformation Behavior of Modified CNS- II F/M Steel. Journal of Iron and Steel Research International, 2012, 19, 60-65.	2.8	6
77	Corrosion Behavior of Ferritic/Martensitic Steels CNS-I and Modified CNS-II in Supercritical Water. Journal of Iron and Steel Research International, 2012, 19, 69-73.	2.8	16
78	Synthesis of TiC/W core–shell nanoparticles by precipitate-coating process. Journal of Nuclear Materials, 2012, 430, 216-220.	2.7	48
79	Effect of Heat Treatment Process on Mechanical Properties and Microstructure of Modified CNS- II F/M Steel. Journal of Iron and Steel Research International, 2011, 18, 65-70.	2.8	5
80	Isothermal Heat Treatment of Wheel Steel with High Cr and Si Contents Based on Microstructure, Mechanical Properties, and Wear Performance. Journal of Materials Engineering and Performance, 0, , 1.	2.5	3
81	Tribological properties of laminate composite brake material for high-speed trains. Tribology Transactions, 0, , 1-15.	2.0	1
82	Wear Behavior of High-Speed Wheel and Rail Steels under Various Hardness Matching. Journal of Materials Engineering and Performance, 0, , .	2.5	2